The influence of Zn^{2+} ions on the local structure and thermochromic properties of $Cu_{1-x}Zn_xMoO_4$ solid solutions

Inga Pudza[a,*], Andris Anspoks[a], Arturs Cintins[a], Aleksandr Kalinko[a,b],
Edmund Welter[b], Alexei Kuzmin[a,**]

[a]*Institute of Solid State Physics, University of Latvia, Kengaraga Street 8, LV-1063
Riga, Latvia*
[b]*Deutsches Elektronen-Synchrotron (DESY) – A Research Centre of the Helmholtz
Association, Notkestrasse 85, D-22607 Hamburg, Germany*

Abstract

The influence of zinc ions on the thermochromic properties of polycrystalline $Cu_{1-x}Zn_xMoO_4$ (x=0.10, 0.50, 0.90) solid solutions was studied by X-ray absorption spectroscopy at the Cu, Zn and Mo K-edges. Detailed structural information on the local environment of metal ions was obtained from the simultaneous analysis of EXAFS spectra measured at three metal absorption edges using the reverse Monte Carlo method. Thermochromic phase transition with the hysteretic behaviour between α and γ phases was observed in $Cu_{0.90}Zn_{0.10}MoO_4$ solid solution. It was found that the local environment of molybdenum ions is most susceptible to the substitution of copper for zinc and, upon cooling, transforms from tetrahedral MoO_4 to distorted octahedral MoO_6.

*Corresponding author
**Corresponding author
  Email addresses: inga.pudza@cfi.lu.lv (Inga Pudza), a.kuzmin@cfi.lu.lv
(Alexei Kuzmin)

1. Introduction

Thermochromic materials change their colour in dependence on temperature but the nature of this effect may have a different origin [1, 2, 3]. In solid inorganic materials, a gradual colour change may occur due to the band gap variation induced by lattice expansion/contraction, while a distinct colour change may take place upon a phase transition affecting the material structure. Both types of thermochromic behaviour are found in copper molybdate $(CuMoO_4)$ [4, 5, 6, 7]. Moreover, it has been demonstrated that replacing molybdenum with tungsten or copper with other divalent metals makes it possible to change the thermochromic response [5, 8, 9, 10, 11, 12, 13]. Thermochromic properties have recently also been found in other molybdates such as $NiMoO_4$ [14] and $CoMoO_4$ [15].

At ambient pressure, pure $CuMoO_4$ exists in two triclinic (space group $P\bar{1}$) phases: high-temperature green α-$CuMoO_4$ and low-temperature brownish γ-$CuMoO_4$ [16]. The γ-$CuMoO_4$ (stable also at high pressure) is composed of distorted CuO_6 and MoO_6 octahedra. During the structural phase transition to α-phase, 1/3 of the octahedra CuO_6 transforms to the square-pyramidal CuO_5, and all molybdenum atoms become tetrahedrally coordinated by oxygen atoms. The thermochromic phase transition between α and γ-phases is of the first order and demonstrates a hysteretic behaviour [5, 16, 17].

α-$ZnMoO_4$ has a white color and is isostructural at ambient conditions to α-$CuMoO_4$ [18, 19]. It is composed of distorted ZnO_6 octahedra, ZnO_5 square-pyramids and MoO_4 tetrahedra [18]. The α-phase of $ZnMoO_4$ is stable in the whole temperature range till it decomposes at 1280 K [18, 20].

3

Note that there also exists β-ZnMoO$_4$ phase, which adopts the wolframite structure type with the monoclinic space group $P2/c$, where both Zn and Mo atoms are octahedrally bonded to six oxygen atoms [21, 22].

The proximity of the Cu^{2+} (0.73 Å) and Zn^{2+} (0.74 Å) ionic radii favors a substitution, so that a complete solid solution series Cu$_{1-x}$Zn$_x$MoO$_4$ ($0 \leq x \leq 1$) exists [20, 23]. Diffraction data reported in [20] show that Zn content higher than $\sim$17.5% leads to a phase similar to α-ZnMoO$_4$.

The substitution of copper with zinc produces a strong effect on thermochromic properties of copper molybdate by tuning its band gap from 2.78 eV in α-CuMoO$_4$ to 3.6 eV in α-ZnMoO$_4$ [24].

Magnetic susceptibility measurements of Cu$_{1-x}$Zn$_x$MoO$_4$ ($0 \leq x \leq 0.1$) reported in [25] indicate a shift of $\alpha \leftrightarrow \gamma$ phase transition hysteresis to the lower temperatures by about 75 K with increasing Zn^{2+} content.

Yanase *et al.* [13] studied the thermochromic phase transition in the Cu$_{1-x}$Zn$_x$Mo$_{0.94}$W$_{0.06}$O$_4$ solid solutions with an even smaller amount of Zn ($0 \leq x \leq 0.05$). The results show that the substitution of Cu^{2+} with Zn^{2+} reduces the phase transition temperature of CuMo$_{0.94}$W$_{0.06}$O$_4$ [10]. For instance, the Zn content of $x=0.01$ induces the largest colour change in the temperature range of 303–343 K in the visible region due to an increase of the γ-to-α phase transition temperature [13].

A deeper understanding of the relationship between crystal structure and thermochromic properties in Cu$_{1-x}$Zn$_x$MoO$_4$ solid solutions requires detailed knowledge of the short-range order variations upon transition metal ion substitution and temperature change. X-ray absorption spectroscopy (XAS) is a suitable tool to address this problem because it provides information about

the local environment around atoms of a specific type. However, the large number of parameters required to describe such complex and low-symmetric molybdate structures makes the conventional extended X-ray absorption fine structure (EXAFS) analysis ineffective. At the same time, the EXAFS analysis based on the reverse Monte-Carlo (RMC) method coupled with an evolutionary algorithm (EA) approach [26] is an effective method that provides the possibility of obtaining a reliable single structural model by fitting EXAFS spectra from several absorption edges simultaneously.

Indeed, the RMC/EA method has been used by us in the past to demonstrate the sensitivity of XAS to the local structure variations in $CuMo_{1-x}W_xO_4$ upon the thermochromic phase transition [27]. Moreover, the hysteretic behaviour of the transition has been evidenced by the analysis of the Mo K-edge X-ray absorption near-edge structure (XANES) and EXAFS [17, 28, 27] and the W L_3-edge high-energy resolution fluorescence detected XANES (HERFD-XANES) [29].

In this study, we applied the temperature-dependent XANES/EXAFS spectroscopy at the Cu, Zn and Mo K-edges to investigate the influence of zinc ions on the local structure and lattice dynamics of $ZnMoO_4$ and $Cu_{1-x}Zn_xMoO_4$ (x=0.10, 0.50, 0.90) solid solutions. The hysteretic thermochromic phase transition between α and γ phases was found only in $Cu_{0.90}Zn_{0.10}MoO_4$ and is explained by the instability of molybdenum coordination under lattice volume change induced by the substitution of copper with zinc and temperature.

2. Experimental details and data analysis

Polycrystalline $Cu_{1-x}Zn_xMoO_4$ (x=0.10, 0.50, 0.90) solid solutions and pure $CuMoO_4$ were synthesized using solid-state reaction method by heating a mixture of CuO, ZnO and MoO_3 powders in a stoichiometric amount at 650°C in air for 8 hours, followed by natural cooling to room temperature. Pure α-$ZnMoO_4$ was synthesized also by solid-state method but a mixture of ZnO and MoO_3 powders was heated for 15 hours. The colour of the resulting samples changes from white (x=1) to greenish (x=0.1) with intermediate pale green colours.

The phase purity of all samples was controlled by X-ray diffraction (XRD). The XRD patterns (Fig. 1) were obtained by a benchtop Rigaku MiniFlex 600 diffractometer with Bragg-Brentano θ-2θ geometry equipped with the 600 W Cu anode (Cu Kα radiation) X-ray tube operated at 40 kV and 15 mA. The obtained patterns of solid solutions are in agreement with the literature data [20, 23]. The contribution of the starting oxide components was not observed which indicates the full completion of the synthesis.

The X-ray absorption experiments were conducted at HASYLAB PETRA III P65 undulator beamline [30] as a function of temperature (from 10 K to 300 K) and sample composition. The PETRA III storage ring operated at E=6.08 GeV and current I=120 mA in top-up 480 bunch mode. The harmonic rejection was achieved by uncoated (Cu/Zn K-edges) and Rh-coated (Mo K-edge) silicon plane mirrors. Fixed exit Si(111) and Si(311) monochromators were used. The X-ray absorption spectra at the Cu (8979 eV), Zn (9659 eV) and Mo (20000 eV) K-edges were collected in transmission mode using two ionisation chambers. The examined powders were gently milled in

an agate mortar and deposited on the Millipore membrane. The temperature-dependent measurements were performed using the Oxford Instruments liquid helium flow cryostat, and the sample temperature was stabilized at each temperature for $\sim$20 min. The $Cu_{0.90}Zn_{0.10}MoO_4$ sample was measured on heating from 10 K to 300 K and on cooling from 300 K to 100 K. All other samples were measured only on heating from 10 K to 300 K.

Temperature-dependence of the Mo K-edge X-ray absorption near-edge structure (XANES) in $Cu_{0.90}Zn_{0.10}MoO_4$ was observed similar to our previous findings for pure $CuMoO_4$ [17], indicating the change in molybdenum coordination. Therefore, its linear combination analysis (LCA) was performed using one of the low-temperature (50 K) and the highest temperature (300 K) XANES spectra as references. The analysis was done using the Athena package [31] in the energy range from 19985 eV to 20015 eV. The obtained results are shown in Fig. 2, where the hysteretic behaviour of the fraction of the α-phase (300 K) is well observed.

Temperature-dependent experimental Cu, Zn and Mo K-edge EXAFS $\chi(k)k^2$ spectra of $Cu_{1-x}Zn_xMoO_4$ were extracted following the conventional procedure [32] using the Athena package [31]. The EXAFS spectra and their Fourier transforms (FTs) at selected temperatures for several samples are shown in Fig. 3. The Zn K-edge EXAFS of $Cu_{0.90}Zn_{0.10}MoO_4$ was excluded from the analysis due it was corrupted by glitches. The FTs were calculated in the k-space range of 1.3–12.0 Å^{-1} (for Cu K-edge), 2.3–14.0 Å^{-1} (for Zn K-edge) and 2.4–15.0 Å^{-1} (for Mo K-edge). The FTs were not corrected for the backscattering phase shift of atoms; therefore, the positions of all peaks are shifted to smaller distances relative to their crystallographic values.

3. Reverse Monte-Carlo simulations

The structural information encoded in the experimental EXAFS data was extracted by the reverse Monte-Carlo calculations with an evolutionary algorithm approach (RMC/EA), as implemented in the EvAX code [26]. The RMC/EA method involves the random changes of atomic coordinates within a three-dimensional structure model of the material, thus minimizing the difference between theoretically calculated configuration-averaged and experimental EXAFS spectra. The contributions from the structural and thermal disorder in the material, as well as multiple-scattering effects, are taken into account. Moreover, the method allows one to perform simultaneous fitting of EXAFS data at several absorption edges, which is required to obtain a reliable structure model for such complex materials as solid solutions [27, 33, 34].

Initial structure models for the RMC/EA calculations were constructed based on diffraction data [16, 18, 23] by randomly substituting Zn atoms with Cu and vice versa, keeping the stoichiometric ratio of the elements in the supercell ($4a \times 4b \times 4c$) containing 2304 atoms. Several random configurations were simulated. In the case of $Cu_{0.90}Zn_{0.10}MoO_4$, structure models based on both α-$CuMoO_4$ and γ-$CuMoO_4$ structures were examined, and the relaxed α-phase gave a slightly better fit than the γ-phase for all examined temperatures.

During RMC/EA simulation, all atoms in the supercell were randomly displaced at each iteration with the maximum allowed displacement of 0.4 Å. The configuration-averaged EXAFS spectra at the Cu, Zn and Mo K-edges were calculated using the *ab initio* self-consistent real-space multiple-scattering

(MS) FEFF8.5L code [35] taking into account multiple-scattering contributions up to the 5th order. The complex energy-dependent exchange-correlation Hedin-Lundqvist potential was employed to account for inelastic effects [36]. The amplitude scaling parameter S_0^2 was set to 1. The comparison between the experimental and theoretical EXAFS spectra was carried out in direct (R) and reciprocal (k) space simultaneously using the Morlet wavelet transform [37]. The convergence of each RMC simulation was achieved after several thousand iterations. At least three RMC/EA simulations with different sequences of pseudo-random numbers were performed for each experimental data set. The resulting structure models describe well the experimental EXAFS data for all absorption edges (Fig. 4).

The final atomic configurations were used to calculate the partial radial distribution functions RDFs $g(R)$ for metal–oxygen and metal–metal atom pairs. The widths of RDFs (the variance of interatomic distances) can be described with the mean-square relative displacement factors (MSRDs). They were evaluated directly from atomic coordinates by the median absolute deviation (MAD) method [38]. Information on interatomic interactions was obtained by analysing the temperature dependencies of the MSRD factors σ^2, which equals to a sum of thermal σ_{th}^2 and static σ_{st}^2 disorder. The temperature dependence of MSRDs was also described by the correlated Einstein model [39].

4. Results and discussion

4.1. Mo K-edge XANES analysis

Temperature-dependent normalized Mo K-edge XANES spectra of $Cu_{0.90}Zn_{0.10}MoO_4$ are shown in Fig. 2. The pre-peak just above the Fermi level corresponds to the $1s(Mo) \rightarrow 4d(Mo) + 2p(O)$ transition. The linear combination analysis (LCA) of the Mo K-edge XANES was performed in the temperature range from 20 to 300 K. In analogy with pure $CuMoO_4$ [17, 27], we assume that $Cu_{0.90}Zn_{0.10}MoO_4$ exists in α-phase at 300 K, while in γ-phase at 20 K. Note that the sample colour changes from green to brownish after treatment in liquid nitrogen ($\sim$77 K) and returns to green after heating up to 300 K as shown in Fig. 2.

A fraction of the α-phase in $Cu_{0.90}Zn_{0.10}MoO_4$ at different temperatures is shown in Fig. 2 and demonstrates hysteresis behavior on cooling and heating. Notably that the phase transition hysteresis in $Cu_{0.90}Zn_{0.10}MoO_4$ is shifted to lower temperatures compared to pure $CuMoO_4$ by about 25 K. At the same time, the variation of the pre-edge peak for $Cu_{0.90}Zn_{0.10}MoO_4$ is not as pronounced as for $CuMoO_4$ reported in [17] indicating on slightly different molybdenum local environment at low temperatures. Based on XANES data, the transition from the α to γ-phase occurs in $Cu_{0.90}Zn_{0.10}MoO_4$ between $\sim$175 K and $\sim$100 K upon cooling, whereas the transition from the γ to α phase begins above $\sim$200 K and ends at $\sim$250 K.

4.2. Experimental EXAFS data

Experimental Cu, Zn and Mo K-edge EXAFS spectra $\chi(k)k^2$ of $Cu_{1-x}Zn_xMoO_4$ together with their FTs are compared in Fig. 3. The first peak located at

about 1-2 Å in FTs is due to the contribution from the first coordination shell formed by oxygen atoms. More distant FT peaks originate from single-scattering contributions of outer coordination shells and multiple-scattering effects. The amplitude of the FT peaks changes upon temperature variation due to the thermal disorder effect. However, contributions up to ∼6-7 Å can be observed even at 300 K.

While the temperature-dependence at the Mo K-edge (especially at low-k values) for samples with $x \geq 0.50$ is very weak, significant changes occur in the first coordination shell of molybdenum in $Cu_{0.90}Zn_{0.10}MoO_4$ sample. Indeed, the amplitude of the FT peak at 1.3 Å increases slightly on heating suggesting the less distorted local environment of molybdenum at 300 K (Fig. 3(f)). Such behaviour is similar to the molybdenum change from octahedral to tetrahedral coordination during the γ-to-α phase transition in pure $CuMoO_4$ [28].

Comparing EXAFS spectra at the Cu and Zn K-edges, one can see that the local environment of zinc atoms exhibits a stronger temperature dependence than that of copper atoms. The damping of the Zn K-edge EXAFS oscillations increases noticeably at high-k values with temperature increase due to enhanced thermal disorder.

4.3. Results of RMC/EA simulations

Detailed structural models were extracted from the experimental EXAFS spectra using RMC/EA calculations taking into account simultaneously two (in $ZnMoO_4$ and $Cu_{0.90}Zn_{0.10}MoO_4$) or three (in $Cu_{1-x}Zn_xMoO_4$ with x=0.50 and 0.90) metal absorption edges. An example of the obtained EXAFS fits, along with corresponding Fourier and Wavelet transforms of the experimen-

tal and theoretical EXAFS spectra, are shown in Fig. 4 on the example of $Cu_{0.50}Zn_{0.50}MoO_4$ sample. Good agreement between the experimental and simulated data was achieved for all three metal absorption edges at all temperatures. Note that the contribution from the first coordination shell of metal atoms dominates EXAFS, FT and WT signals, however, the outer shells are also detectable up to 5-6 Å.

Final sets of atomic coordinates obtained in the RMC/EA simulations were used to calculate partial radial distribution functions (RDFs) around absorbing atoms. They are reported up to 6 Å for $ZnMoO_4$ at 10 K and 300 K in Fig. 5. As one can see, the first coordination shell is well separated, while outer shells overlap strongly. Therefore, we will concentrate further on the analysis and discussion of the first coordination shell only.

Temperature dependence of partial RDFs $g_{Zn-O}(R)$, $g_{Cu-O}(R)$, and $g_{Mo-O}(R)$ for $ZnMoO_4$ and $Cu_{1-x}Zn_xMoO_4$ is shown in Fig. 6.

The RDFs $g_{Cu-O}(R)$ for Cu–O atom pairs have two maxima at $\sim$1.9 Å and $\sim$2.3 Å with a relative area of about 4:2. Strong distortion of the first coordination shell of copper ions is caused by the first-order Jahn-Teller effect due to the $Cu^{2+}[3d^9]$ electronic configuration. The distribution of the nearest four oxygen atoms, located in the plane of the CuO_6 octahedron/CuO_5 square-pyramid, has a rather weak dependence on temperature due to strong Cu–O bonds. The two axial oxygen atoms contribute to the second broad peak of the RDF. Averaged Zn–O and Cu–O interatomic distances calculated from atomic coordinates in the structural models are shown with vertical dashed lines in Fig. 6 for $ZnMoO_4$ and $Cu_{0.90}Zn_{0.10}MoO_4$, respectively. One can see that during heating, the longest Cu–O bond slightly lengthens.

The local environment of zinc ions differs from that of copper, since Zn^{2+} has an electronic configuration $3d^{10}$ and, thus, the Jahn-Teller distortion is absent. The distribution $g_{Zn-O}(R)$ can be characterized with one asymmetric peak with a maximum at about 2.06 Å, due to both ZnO_6 octahedron/ZnO_5 square-pyramid are slightly deformed.

The distribution $g_{Mo-O}(R)$ of the nearest four oxygen atoms, forming MoO_4 tetrahedron with R(Mo–O)≈1.77 Å, is rather narrow and has a weak dependence on temperature due to strong Mo–O bonds. The RDFs $g_{Mo-O}(R)$ in pure α-$ZnMoO_4$ and $Cu_{1-x}Zn_xMoO_4$ solid solutions with x=0.50 and 0.90 remain nearly unchanged in the temperature range of 20-300 K. At the same time, some variation of the $g_{Mo-O}(R)$ upon temperature increase is observed in $Cu_{0.90}Zn_{0.10}MoO_4$ and related to structural changes.

4.4. MSRD factors

The widths of RDFs can be characterized by the MSRD factors σ^2. However, due to the distorted environment of metal ions, only the groups of nearest oxygen atoms, which are responsible for the main peak in partial RDFs in Fig. 6, have been considered in the evaluation of σ^2.

The calculated MSRDs are plotted as a function of temperature and composition in Fig. 7. The temperature dependencies were fitted with the correlated Einstein model [39], and the static disorder factors σ_{st} were estimated.

Similar to the result of the Mo K-edge XANES analysis (Fig. 2), the temperature-dependence of Mo–O distances in $Cu_{0.90}Zn_{0.10}MoO_4$ shows hysteretic behaviour (Fig. 7(a)). Note that the MSRD values σ^2(Mo–O) at temperatures below 250 K are much smaller than for isostructural low-temperature γ-$CuMoO_4$. At the same time, the value of the MSRD factor

at 300 K is close to that in high-temperature α-CuMoO$_4$.

No hysteresis was found for pure ZnMoO$_4$ and Cu$_{1-x}$Zn$_x$MoO$_4$ solid so-lutions with x=0.50 and 0.90. In fact, small values and weak temperature dependence of their MSRDs indicate strong Mo–O bonding, which is charac-teristic of MoO$_4$ tetrahedral coordination. The estimated Einstein frequency is equal to about ω_E=111±52 THz.

The MSRDs values σ^2(Cu–O) for the four shortest Cu–O bonds are close in all Cu$_{1-x}$Zn$_x$MoO$_4$ solid solutions and CuMoO$_4$ from [27] within error bars (Fig. 7(c)). Their Einstein frequencies are in the range of ω_E=78±39 THz.

The MSRD values σ^2(Zn–O) for groups of the nearest four (Zn–O(4)) or five (Zn–O(5)) oxygen atoms show weak dependence on the composition (Fig. 7(d)) being close in α-ZnMoO$_4$ and Cu$_{1-x}$Zn$_x$MoO$_4$ samples with x=0.90 and 0.50. The calculated Einstein frequencies are equal to ω_E=68±10 THz when one considers only four nearest oxygen atoms and ω_E=52±4 THz when the fifth oxygen atom is additionally included.

The composition dependence of static distortions around metal ions in Cu$_{1-x}$Zn$_x$MoO$_4$ solid solutions can be evaluated based on the values of σ^2_{st} for the nearest four Cu–O, Zn–O and Mo–O atom pairs (Fig. 7(b)).

The σ^2_{st} values for the Mo–O bonds reveal that the static distortions are much larger in the low-temperature γ-CuMoO$_4$ than in the low-temperature phase of Cu$_{0.90}$Zn$_{0.10}$MoO$_4$, both having distorted octahedral coordination of molybdenum ions.

Note that the 50% of α-Cu$_{0.90}$Zn$_{0.10}$MoO$_4$ transforms to the low-temperature phase during cooling at $T_{1/2C}$ ≈125 K (134 K from XANES in Fig. 2) and returns on heating at $T_{1/2H}$ ≈225 K (Fig. 7(a)). Both $T_{1/2C}$ and $T_{1/2H}$ val-

ues are shifted to lower temperatures in comparison to pure $CuMoO_4$, where $T_{1/2C} \approx$143-155 K and $T_{1/2H} \approx$255 K (Fig. 2 and [17]). Thus, the substitution of Cu^{2+} ions with Zn^{2+} ions stabilizes the α-phase, which is natural for α-$ZnMoO_4$.

The tetrahedral coordination of molybdenum ions at room-temperature in α-$CuMoO_4$, α-$ZnMoO_4$ and α-$Cu_{1-x}Zn_xMoO_4$ solid solutions is responsible for small values of σ_{st}^2 for Mo–O bonds in Fig. 7(b). The distorted octahedral environment of zinc ions results in larger values of σ_{st}^2 for the Zn–O bonds and is almost constant at large $x \geq 0.5$. An increase of σ_{st}^2 for the Cu–O bonds can be related to the role played by copper ions upon increasing x. Static distortions are smallest in pure α-$CuMoO_4$, increase upon a formation of the solid solution with a maximum at $x=0.50$ and remain constant for a small amount of copper ($x>0.50$) when the structure is determined by the zinc sublattice.

To conclude, the local environment of molybdenum ions in $Cu_{1-x}Zn_xMoO_4$ solid solutions can be significantly affected by the substitution of copper with zinc, since the electronic configurations of the two 3d-ions differ significantly. Indeed, the 3d(Zn^{2+})-subshell is filled, while the $3d^9$ configuration of Cu^{2+} makes it subject to the first-order Jahn-Teller distortion leading to tetragonal deformation of CuO_6 octahedra. The substitution modifies the electronic structure of molybdate by increasing its band gap [24] and leads to a disappearance of thermochromic properties, which are closely related to the local structure of molybdenum ions. The coordination of molybdenum ions changes from distorted octahedral at low-temperature in γ-$Cu_{0.90}Zn_{0.10}MoO_4$ solid solution to tetrahedral in α-$Cu_{0.90}Zn_{0.10}MoO_4$ above 250 K, similar to

temperature or pressure-induced the γ-to-α phase transitions in CuMoO$_4$ [16]. At the same time, molybdenum ions have always tetrahedral coordination in α-Cu$_{1-x}$Zn$_x$MoO$_4$ with $x>0.10$ and α-ZnMoO$_4$.

5. Conclusions

The influence of zinc ions on the thermochromic properties of polycrystalline Cu$_{1-x}$Zn$_x$MoO$_4$ (x=0.10, 0.50, 0.90) solid solutions was studied by X-ray absorption spectroscopy at the Cu, Zn and Mo K-edges. The analysis of XANES and EXAFS spectra revealed that the substitution of Cu^{2+} ions with Zn^{2+} ions stabilizes the α-phase, which is natural for α-ZnMoO$_4$, and significantly affects the temperature of the thermochromic phase transition in the materials.

We found that among sampled solid solutions, only Cu$_{0.90}$Zn$_{0.10}$MoO$_4$ exhibited a thermochromic phase transition between α and γ phases with the hysteretic behaviour. This result is in agreement with that of the previous work [25].

To understand the structural origin of the thermochromic phase transition in Cu$_{0.90}$Zn$_{0.10}$MoO$_4$, a detailed analysis of the mean-square relative displacement factors for metal–oxygen bonds in the first coordination shell was performed. We found that the substitution of copper with zinc affects strongly the local environment of molybdenum ions. This result can be explained by the instability of molybdenum coordination, which is tetrahedral in α-Cu$_{0.90}$Zn$_{0.10}$MoO$_4$ solid solution at room temperature but changes to distorted octahedral under lattice contraction at low-temperature in γ-Cu$_{0.90}$Zn$_{0.10}$MoO$_4$, similar to temperature or pressure-induced the α-to-γ

phase transitions in $CuMoO_4$ [16].

Thus, tuning the thermochromic properties of $CuMoO_4$ by doping with zinc may find useful applications for controlling storage conditions in the low-temperature range.

Acknowledgements

Data availability

The raw/processed data required to reproduce these findings cannot be shared at this time due to technical or time limitations.

References

[1] J. H. Day, Thermochromism of inorganic compounds, Chem. Rev. 68 (1968) 649–657. `doi:10.1021/cr60256a001`.

[2] P. Kiri, R. B. G. Hyett, Solid state thermochromic materials, Adv. Mat. Lett. 1 (2010) 86–105. `doi:10.5185/amlett.2010.8147`.

[3] Y. Wang, E. L. Runnerstom, D. J. Milliron, Switchable materials for smart windows, Annu. Rev. Chem. Biomol. Eng. 7 (2016) 283–304. `doi:10.1146/annurev-chembioeng-080615-034647`.

[4] G. Steiner, R. Salzer, W. Reichelt, Temperature dependence of the optical properties of $CuMoO_4$, Fresenius J. Anal. Chem. 370 (2001) 731–734. `doi:10.1007/s002160000630`.

[5] M. Gaudon, C. Carbonera, A. E. Thiry, A. Demourgues, P. Deniard, C. Payen, J. F. Létard, S. Jobic, Adaptable thermochromism in the $CuMo_{1-x}W_xO_4$ series ($0 \leq x < 0.1$): A behavior related to a first-order phase transition with a transition temperature depending on x, Inorg. Chem. 46 (2007) 10200–10207. `doi:10.1021/ic701263c`.

[6] I. Jonane, A. Anspoks, G. Aquilanti, A. Kuzmin, High-temperature X-ray absorption spectroscopy study of thermochromic copper molybdate, Acta Mater. 179 (2019) 26–35. `doi:10.1016/j.actamat.2019.06.034`.

[7] N. Joseph, J. Varghese, M. Teirikangas, H. Jantunen, A temperature-responsive copper molybdate polymorph mixture near to water boiling point by a simple cryogenic quenching route, ACS Appl. Mater. Interfaces 12 (2020) 1046–1053. `doi:10.1021/acsami.9b17300`.

[8] M. Gaudon, P. Deniard, A. Demourgues, A. E. Thiry, C. Carbonera, A. Le Nestour, A. Largeteau, J. F. Létard, S. Jobic, Unprecedented "one-finger-push"-induced phase transition with a drastic color change in an inorganic material, Adv. Mater. 19 (2007) 3517–3519. doi:10.1002/adma.200700905.

[9] M. Gaudon, C. Riml, A. Turpain, C. Labrugere, M. H. Delville, Investigation of the chromic phase transition of $CuMo_{0.9}W_{0.1}O_4$ induced by surface protonation, Chem. Mater. 22 (2010) 5905–5911. doi:10.1021/cm101824d.

[10] I. Yanase, T. Mizuno, H. Kobayashi, Structural phase transition and thermochromic behavior of synthesized W-substituted $CuMoO_4$, Ceram. Int. 39 (2013) 2059–2064. doi:10.1016/j.ceramint.2012.08.059.

[11] V. Blanco-Gutierrez, L. Cornu, A. Demourgues, M. Gaudon, $CoMoO_4/CuMo_{0.9}W_{0.1}O_4$ mixture as an efficient piezochromic sensor to detect temperature/pressure shock parameters, ACS Appl. Mater. Interfaces 7 (2015) 7112–7117. doi:10.1021/am508652h.

[12] L. Robertson, N. Penin, V. Blanco-Gutierrez, D. Sheptyakov, A. Demourgues, M. Gaudon, $CuMo_{0.9}W_{0.1}O_4$ phase transition with thermochromic, piezochromic, and thermosalient effects, J. Mater. Chem. C 3 (2015) 2918–2924. doi:10.1039/C4TC02463J.

[13] I. Yanase, R. Koda, R. Kondo, R. Taiji, Improvement of thermochromic property at low temperatures of $CuMo_{0.94}W_{0.06}O_4$ by Zn substitu-

tion, J. Therm. Anal. Calorim. 140 (2019) 2203–2214. `doi:10.1007/` `s10973-019-09025-7`.

[14] M. V. da Silva, D. F. M. de Oliveira, H. S. Oliveira, K. P. F. Siqueira, Influence of temperature on the structural and color properties of nickel molybdates, Mater. Res. Bull. 122 (2020) 110665. `doi:10.1016/j.` `materresbull.2019.110665`.

[15] R. K. S. Costa, S. C. Teles, K. P. F. Siqueira, The relationship between crystal structures and thermochromism in $CoMoO_4$, Chem. Pap. 75 (2020) 237–248. `doi:10.1007/s11696-020-01294-z`.

[16] M. Wiesmann, H. Ehrenberg, G. Miehe, T. Peun, H. Weitzel, H. Fuess, $p-T$ phase diagram of $CuMoO_4$, J. Solid State Chem. 132 (1997) 88–97. `doi:10.1006/jssc.1997.7413`.

[17] I. Jonane, A. Cintins, A. Kalinko, R. Chernikov, A. Kuzmin, X-ray absorption near edge spectroscopy of thermochromic phase transition in $CuMoO_4$, Low Temp. Phys. 44 (2018) 434–437. `doi:10.1063/1.` `5034155`.

[18] S. Abrahams, Crystal structure of the transition-metal molybdates and tungstates. III. Diamagnetic α-$ZnMoO_4$, J. Chem. Phys. 46 (1967) 2052–2063. `doi:10.1063/1.1841001`.

[19] P. Yadav, E. Sinha, Structural, photophysical and microwave dielectric properties of α-$ZnMoO_4$ phosphor, J. Alloys Compd. 795 (2019) 446–452. `doi:10.1016/j.jallcom.2019.05.019`.

[20] U. Steiner, W. Reichelt, S. Däbritz, Chemischer Transport von Mischkristallen im System $CuMoO_4/ZnMoO_4$, Z. Anorg. Allg. Chem. 629 (2003) 116–122. `doi:10.1002/zaac.200390002`.

[21] L. Cavalcante, E. Moraes, M. Almeida, C. Dalmaschio, N. Batista, J. Varela, E. Longo, M. Siu Li, J. Andres, A. Beltrán, A combined theoretical and experimental study of electronic structure and optical properties of β-$ZnMoO_4$ microcrystals, Polyhedron 54 (2013) 13–25. `doi:10.1016/j.poly.2013.02.006`.

[22] O. Mtioui-Sghaier, R. Mendoza-Meroño, L. Ktari, M. Dammak, S. García-Granda, Redetermination of the crystal structure of β-zinc molybdate from single-crystal X-ray diffraction data, Acta Crystallogr. E 71 (2015) i6–i7. `doi:10.1107/S205698901501186X`.

[23] W. Reichelt, T. Weber, T. Söhnel, S. Däbritz, Mischkristallbildung im System $CuMoO_4/ZnMoO_4$, Z. Anorg. Allg. Chem. 626 (2000) 2020–2027. `doi:10.1002/1521-3749(200009)626:9<2020::AID-ZAAC2020>3.0.CO;2-K`.

[24] S. K. Tiwari, A. Singh, P. Yadav, B. K. Sonu, R. Verma, S. Rout, E. Sinha, Structural and dielectric properties of Cu-doped α-$ZnMoO_4$ ceramic system for enhanced green light emission and potential microwave applications, J. Mater. Sci.: Mater. Electron. (2020). `doi:10.1007/s10854-020-04225-6`.

[25] T. Asano, T. Nishimura, S. Ichimura, Y. Inagaki, T. Kawae, T. Fukui, Y. Narumi, K. Kindo, T. Ito, S. Haravifard, et al., Magnetic ordering and

tunable structural phase transition in the chromic compound $CuMoO_4$, J. Phys. Soc. Jpn. 80 (2011) 093708. `doi:10.1143/JPSJ.80.093708.`

[26] J. Timoshenko, A. Kuzmin, J. Purans, EXAFS study of hydrogen intercalation into ReO_3 using the evolutionary algorithm, J. Phys.: Condens. Matter 26 (2014) 055401. `doi:10.1088/0953-8984/26/5/055401.`

[27] I. Jonane, A. Cintins, A. Kalinko, R. Chernikov, A. Kuzmin, Low temperature X-ray absorption spectroscopy study of $CuMoO_4$ and $CuMo_{0.90}W_{0.10}O_4$ using reverse Monte-Carlo method, Rad. Phys. Chem. 175 (2020) 108411. `doi:0.1016/j.radphyschem.2019.108411.`

[28] I. Jonane, A. Cintins, A. Kalinko, R. Chernikov, A. Kuzmin, Probing the thermochromic phase transition in $CuMoO_4$ by EXAFS spectroscopy, Phys. Status Solidi B 255 (2018) 1800074. `doi:10.1002/pssb.201800074.`

[29] I. Pudza, A. Kalinko, A. Cintins, A. Kuzmin, Study of the thermochromic phase transition in $CuMo_{1-x}W_xO_4$ solid solutions at the W L_3-edge by resonant X-ray emission spectroscopy, Acta Mater. 205 (2021) 116581. `doi:10.1016/j.actamat.2020.116581.`

[30] E. Welter, R. Chernikov, M. Herrmann, R. Nemausat, A beamline for bulk sample x-ray absorption spectroscopy at the high brilliance storage ring PETRA III, AIP Conf. Proc. 2054 (2019) 040002. `doi:10.1063/1.5084603.`

[31] B. Ravel, M. Newville, ATHENA, ARTEMIS, HEPHAESTUS: data analysis for X-ray absorption spectroscopy using IFEF-

FIT, J. Synchrotron Radiat. 12 (2005) 537–541.   `doi:10.1107/S0909049505012719`.

[32] A. Kuzmin, J. Chaboy, EXAFS and XANES analysis of oxides at the nanoscale, IUCrJ 1 (2014) 571–589. `doi:10.1107/S2052252514021101`.

[33] J. Timoshenko, A. Anspoks, A. Kalinko, A. Kuzmin, Analysis of extended x-ray absorption fine structure data from copper tungstate by the reverse Monte Carlo method, Phys. Scr. 89 (2014) 044006. `doi:10.1088/0031-8949/89/04/044006`.

[34] J. Timoshenko, A. Anspoks, A. Kalinko, I. Jonane, A. Kuzmin, Local structure of multiferroic $MnWO_4$ and $Mn_{0.7}Co_{0.3}WO_4$ revealed by the evolutionary algorithm, Ferroelectrics 483 (2015) 68–74. `doi:10.1080/00150193.2015.1058687`.

[35] A. Ankudinov, B. Ravel, J. Rehr, S. Conradson, Real-space multiple-scattering calculation and interpretation of x-ray-absorption near-edge structure, Phys. Rev. B 58 (1998) 7565. `doi:10.1103/PhysRevB.58.7565`.

[36] L. Hedin, B. I. Lundqvist, Explicit local exchange-correlation potentials, J. Phys. C: Solid State Phys. 4 (1971) 2064. `doi:10.1088/0022-3719/4/14/022`.

[37] J. Timoshenko, A. Kuzmin, Wavelet data analysis of EXAFS spectra, Comput. Phys. Commun. 180 (2009) 920–925. `doi:10.1016/j.cpc.2008.12.020`.

[38] M. Daszykowski, K. Kaczmarek, Y. Vander Heyden, B. Walczak, Robust statistics in data analysis – A review: Basic concepts, Chemom. Intell. Lab. Syst. 85 (2007) 203–219. `doi:10.1016/j.chemolab.2006.06.016.`

[39] E. Sevillano, H. Meuth, J. Rehr, Extended x-ray absorption fine structure Debye-Waller factors. I. Monatomic crystals, Phys. Rev. B 20 (1979) 4908. `doi:10.1103/PhysRevB.20.4908.`
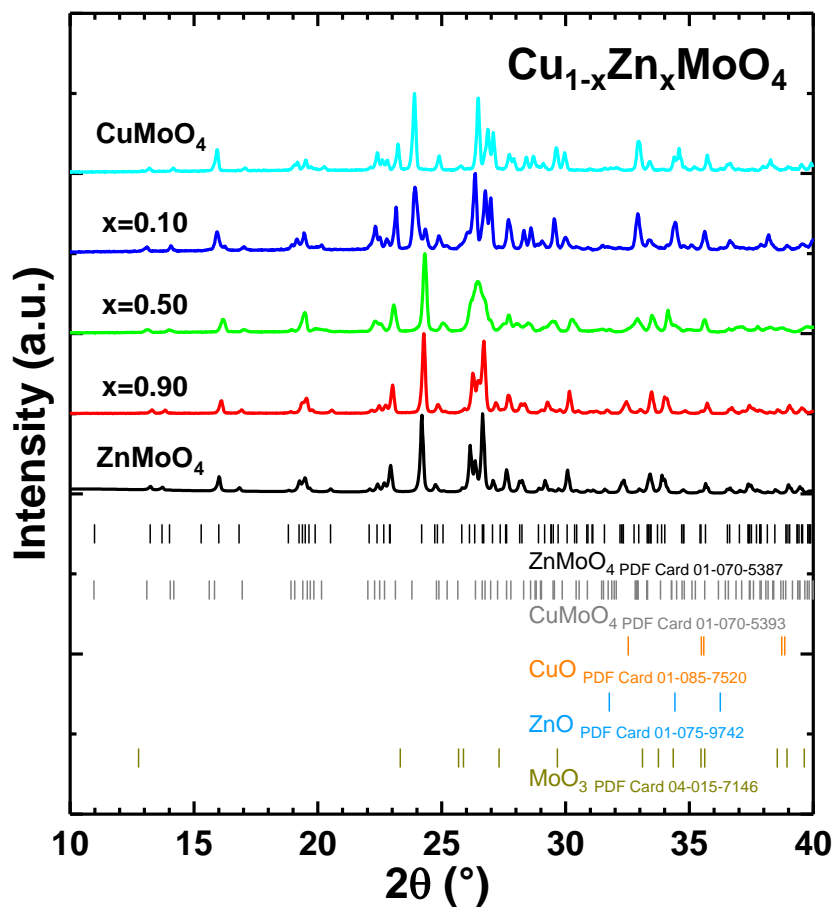
Figure 1: X-ray diffraction patterns of $Cu_{1-x}Zn_xMoO_4$ solid solutions. The standard PDF cards of $ZnMoO_4$ (PDF Card 01-070-5387), $CuMoO_4$ (PDF Card 01-070-5393), CuO (PDF Card 01-085-7520), ZnO (PDF Card 01-075-9742) and MoO_3 (PDF Card 04-015-71446) phases are shown for comparison.
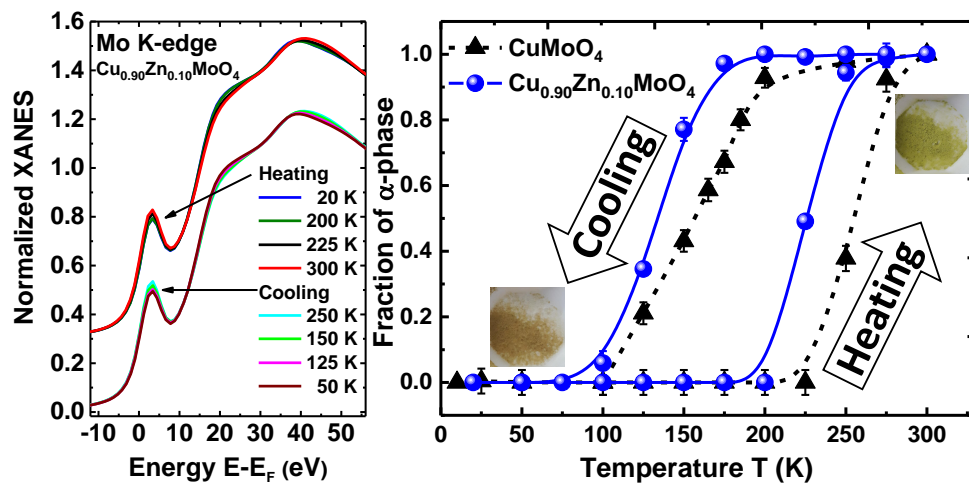
Figure 2: Left panel: Experimental Mo K-edge XANES of $Cu_{0.90}Zn_{0.10}MoO_4$ as a function of temperature during the sample cooling and heating. Right panel: Temperature dependence of the α-phase fraction in $CuMoO_4$ [27] and $Cu_{0.90}Zn_{0.10}MoO_4$ upon heating and cooling. Photographs of the $Cu_{0.90}Zn_{0.10}MoO_4$ sample at 77 K (brownish) and 300 K (green) are also shown.
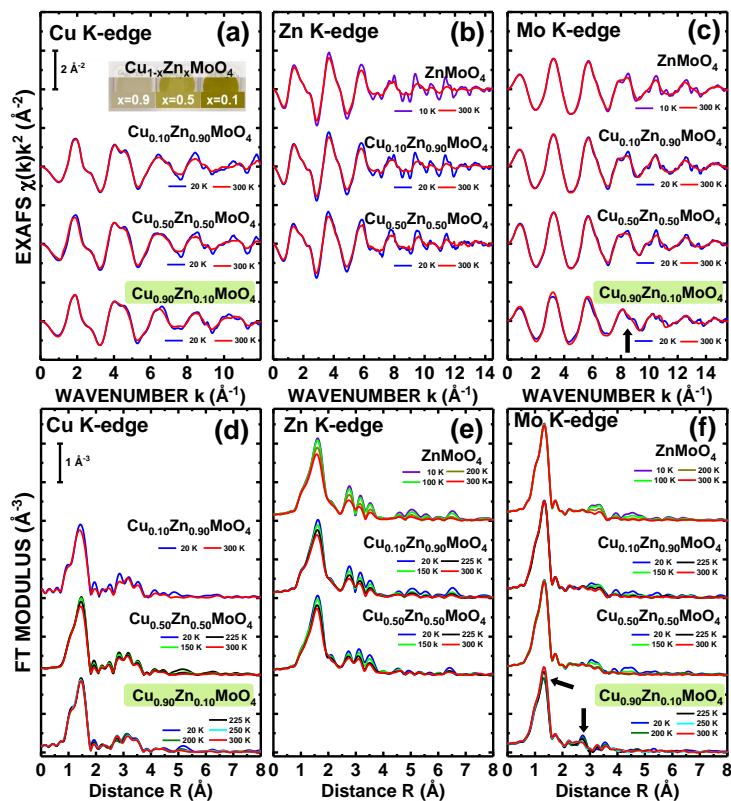
Figure 3: Temperature-dependent experimental Cu, Zn and Mo K-edge EXAFS spectra $\chi(k)k^2$ for $ZnMoO_4$ and $Cu_{1-x}Zn_xMoO_4$ (x=0.10, 0.50, 0.90) at selected temperatures (a-c) and corresponding Fourier transforms (d-f).
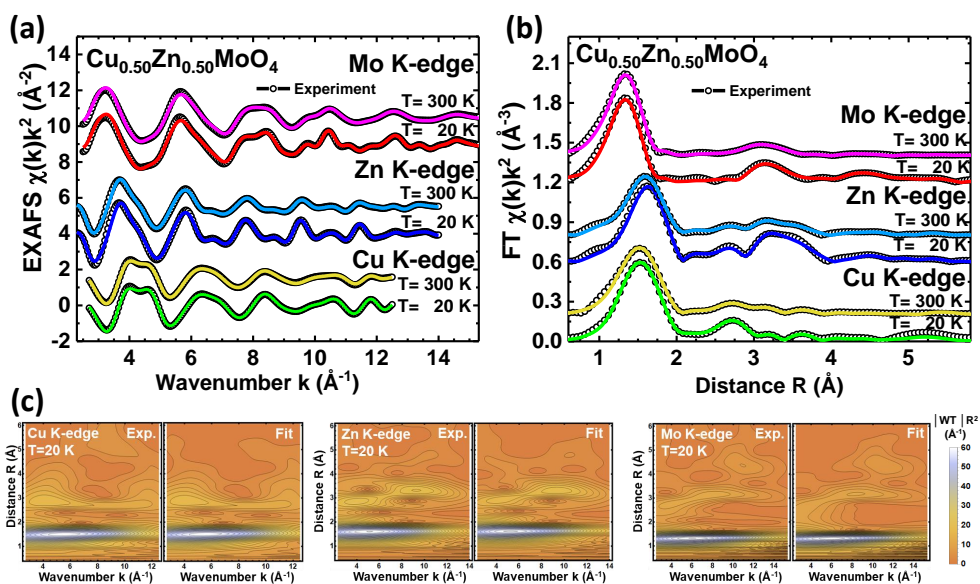
Figure 4: Comparison of the experimental (T=20 and 300 K) and calculated configuration-averaged Cu, Zn and Mo K-edge EXAFS spectra of $Cu_{0.50}Zn_{0.50}MoO_4$ (a) and their Fourier (b) and Morlet wavelet transforms (T=20 K) (c).
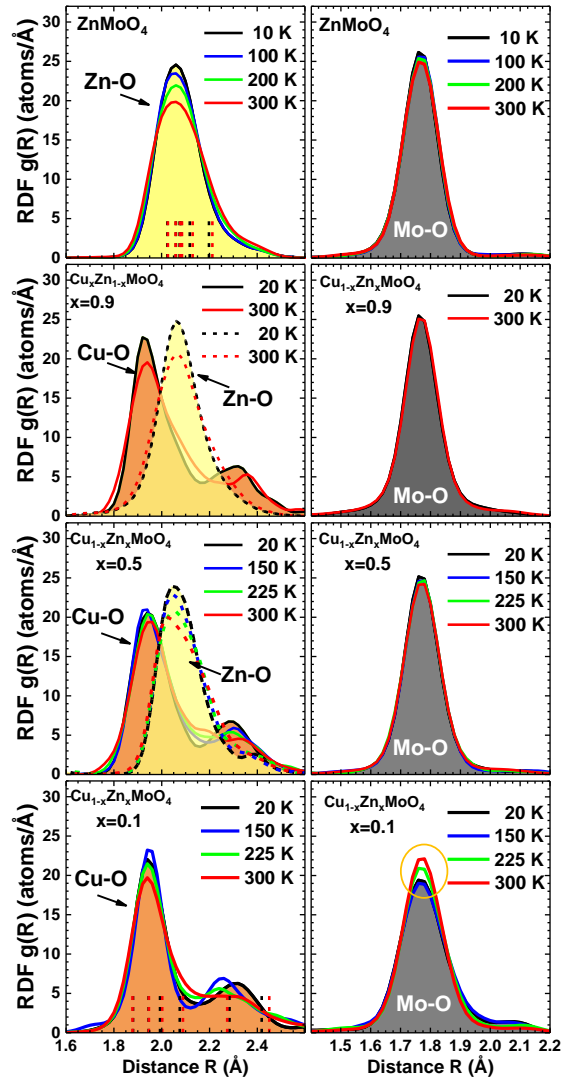
Figure 5: Partial RDFs around zinc and molybdenum atoms in ZnMoO$_4$ at T=10 K and 300 K obtained in RMC/EA simulations. Contributions from different atom pairs are indicated.
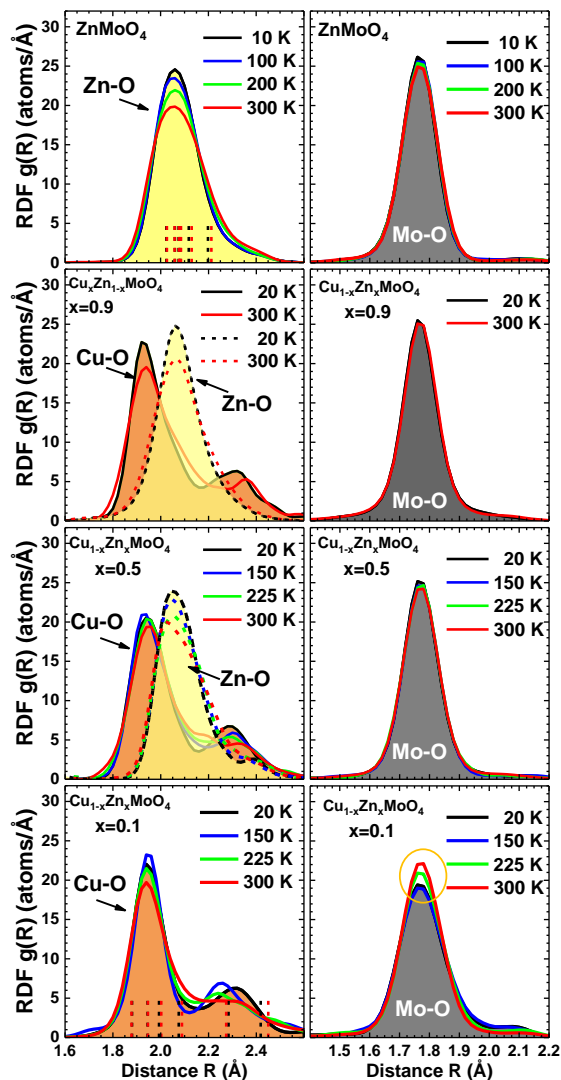
Figure 6: Temperature-dependent partial RDFs $g_{\mathrm{Zn-O}}(R)$, $g_{\mathrm{Cu-O}}(R)$ and $g_{\mathrm{Mo-O}}(R)$ obtained in RMC/EA simulations. Vertical dashed lines in $g_{\mathrm{Zn-O}}(R)$ plot for $\mathrm{ZnMoO_4}$ and $g_{\mathrm{Cu-O}}(R)$ plot for $\mathrm{Cu_{0.90}Zn_{0.10}MoO_4}$ indicate average Zn–O and Cu–O interatomic distances, respectively, at 10 K(20 K) and 300 K (black and red lines, respectively).
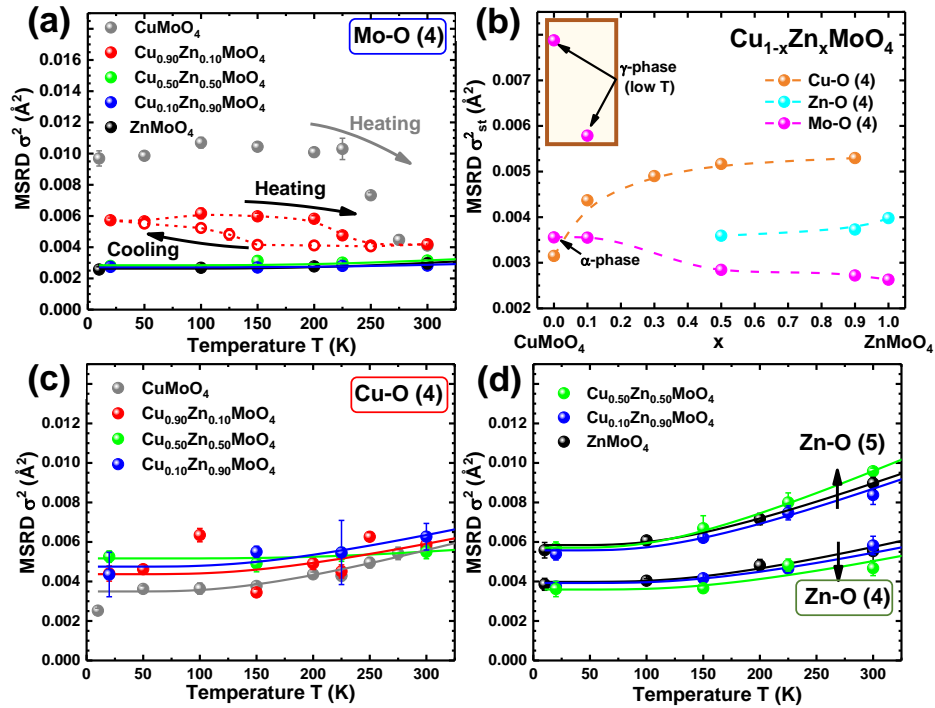
Figure 7: Temperature dependencies of the MSRD factors σ^2, obtained in RMC/EA simulations for metal (Mo, Cu, Zn) and surrounding four nearest oxygen atoms (a, c, d). Additionally MSRD σ^2 calculated for zinc and five nearest oxygens is plotted in panel (d) for comparison. Static disorder term σ_{st}^2 as a function of zinc concentration x in $Cu_{1-x}Zn_xMoO_4$ is shown in panel (b). Solid lines are fits by the correlated Einstein model. Dashed lines are guide for eye.